Available online at www.sciencedirect.com
ScienceDirect
Bioorganic & Medicinal Chemistry 14 (2006) 8359–8365
Bioorganic & Medicinal Chemistry

Structure of C-terminal fragment of merozoite surface protein-1 from *Plasmodium vivax* determined by homology modeling and molecular dynamics refinement

María Luisa Serrano,[a,*] Hilda A. Pérez[b] and J. D. Medina[c]

[a]*Laboratorio de Modelado Molecular, Unidad de Química Medicinal, Facultad de Farmacia, Universidad Central de Venezuela, Caracas 1041-A, Venezuela*
[b]*Laboratorio de Inmunoparasitología, Centro de Microbiología y Biología Celular, IVIC, Apartado 21827, Caracas 1020-A, Venezuela*
[c]*Laboratorio de Síntesis Orgánica y Productos Naturales, Centro de Química, IVIC, Apartado 21827, Caracas 1020-A, Venezuela*

Received 5 July 2006; revised 7 September 2006; accepted 7 September 2006
Available online 10 October 2006

Abstract—One current vaccine candidate against *Plasmodium vivax* targeting asexual blood stage is the major merozoite surface protein-1 of *P. vivax* (PvMSP-1). Vaccine trials with PvMSP-1_{19} and PvMSP-1_{33} have succeeded in protecting monkeys and a large proportion of individuals, naturally exposed to *P. vivax* transmission, develop specific antibodies to PvMSP-1_{19}. This study presents a model for the three-dimensional structure of the C-terminal 19 kDa fragment of *P. vivax* MSP-1 determined by means of homology modeling and molecular dynamics refinement. The structure proved to be consistent with MSP-1_{19} of known crystal or solution structures. The presence of a main binding pocket, well suited for protein–protein interactions, was determined by CASTp. Corrections reported to the sequence of PvMSP-1_{19} Belem strain were also inspected. Our model is currently used as a basis to understand antibody interactions with PvMSP-1_{19}.

1. Introduction

Despite significant efforts over the past 50 years to control malaria, the disease continues to be a major health problem in the tropical world. Human malaria is caused by four *Plasmodium* species, namely, *P. falciparum*, *P. vivax*, *P. malariae*, and *P. ovale*. While *P. falciparum* prevails on the African continent where is primarily blamed for the mortality associated with malaria,[1] *Plasmodium vivax* is the most widespread of the four *Plasmodium* species; it accounts for more than 50% of all malaria cases outside Africa and is responsible for significant morbidity in Central and South America, South-east and South Asia, Papua New Guinea, and parts of Africa with a yearly estimate of 80 million cases.[2] Vaccines to afford protection against *P. falciparum* and *P. vivax* are urgently required. However, the development of an effective malaria vaccine has been challenged by the biological and molecular complexity of *Plasmodium* parasites and, not less important, because protective immunity to malaria is poorly understood. Clinical symptoms of malaria are attributed to the blood-stages of the parasite life cycle ensuing repeated rounds of erythrocyte invasion, intracellular multiplication, and lysis of host erythrocytes. An effective vaccine against the erythrocytic stages of malaria parasites would be expected to limit parasite multiplication rates and thereby reduce morbidity and mortality and spreading of drug resistant parasites. Proteins on the surface of the merozoite (MSP) have been considered a prime target for a blood stage malaria vaccine since they are exposed to potentially effective immune mechanism leading to interruption of the parasite blood cycle. Ten members of the MSP family have been described in *P. falciparum* (PfMSP1-10)[3–10] of which, eight have been recognized in *P. vivax* (PvMSP-1, PvMSP-185, PvMSP-3α, PvMSP-3β, PvMSP3γ, PvMSP-4, PvMSP-5, PvMSP-8, PvMSP-9, and PVMSP-10).[11–17] Among the MSP family, MSP-1 is a leading vaccine candidate.[18,19] Studies performed mainly in *P. falciparum* indicate that MSP-1 is processed by proteolytic cleavage at, or just prior to, merozoite release into 83, 30, 38, and 42 kDa fragments.[20–22] Before completion of erythrocyte invasion,

Keywords: Homology modeling; Molecular dynamics; Malaria; *P. vivax*; MSP-1_{19}.
* Corresponding author. Tel.: +58 212 605 2697; fax: +58 212 605 2707; e-mail: serranol@ucv.ve

0968-0896/$ - see front matter © 2006 Elsevier Ltd. All rights reserved.
doi:10.1016/j.bmc.2006.09.005

the C-terminal 42 kDa fragment, attached to the merozoite surface, is further processed into 33 and 19 kDa fragments with only the 19 kDa fragment being carried into the newly infected erythrocyte.[20,23,24] The 19 kDa polypeptide enclosed two epidermal growth factor (EGF)-like domains and monoclonal antibodies binding MSP-1_{19} has the ability to inhibit the invasion of erythrocytes in vitro.[23,25–27] Immunization with $MSP1_{42}$ and $MSP1_{19}$ have shown to provide partial immunity against the blood stages of *P. falciparum* in *Aotus* monkeys.[19,28,29] Homologue PvMSP-1, a 200 kDa protein expressed on the surface of *P. vivax* merozoite,[11] is also a current vaccine candidate against asexual blood stage. Immunization of *Saimiri* monkeys with a $PvMSP1_{19}$ recombinant fragment derived from the Sal-1 strain of *P. vivax* provided partial protection against *P. vivax* homologous challenge[30,31] and *Aotus* monkeys immunized with a mixture of recombinant polypeptides encoding the PvMSP-1 33 kDa fragment of the *P. vivax* Belem strain developed partial protection against a heterologous strain challenge.[32] Studies on the naturally acquired humoral immune responses against PvMSP-1 showed that PvMSP-1_{19} is the most immunogenic portion of the molecule, being recognized by 64% of the patients from endemic regions in the Brazilian Amazone.[33]

Albeit MSP-1_{19} has long been regarded as a clue component of a MSP-1 malaria-based vaccine, it has been argued that MSP-1_{19} has limited T cell epitopes,[34] MSP-1_{42} being probably a better vaccine since immunodominant T cell epitopes may be located in the upstream 33 kDa fragment.[34] Interestingly, PfMSP-1_{42} vaccine provided better protection than PfMSP-1_{19} against blood stage challenge in *Aotus* monkeys.[19] Recent studies with polypeptides (rPvMSP-1_{14} and rPvMSP-1_{20}) contained in the 33 kDa fragment located within PvMSP-1_{42} indicated that protection against a *P. vivax* blood stage challenge was best achieved when immunizing with a rPvMSP-1_{14}-rPvMSP-1_{20} mixture.[32]

Molecular modeling of the three-dimensional structure of the MSP-1 C-terminal fragment of *P. vivax* could provide a better understanding of how molecular structure relates to biological activity. For example, the structure could assist in the prediction of T and B cell epitopes, help in the identification of prominent antibody binding sites, and anticipate the effect of mutation on immunogenicity using a structure-based approach. To date, the crystal structures of the C-terminal domains of PcMSP-1 (*P. cynomolgi*),[35] PkMSP-1 (*P. knowlesi*)[36], and the solution structure of PfMSP-1 (*P. falciparum*),[37] have been reported. These studies confirmed the presence of two EGF-like domains and revealed the compact integral entity formed by these two domains. The C-terminal region of MSP-1, which represents a conserved segment within this variable molecule, shows high sequence identity within *Plasmodium* species: *P. vivax* shares 84% sequence identity with *P. cynomolgi*, 81% with *P. knowlesi*, and 54% sequence identity with *P. falciparum.*

Here, we propose a model for the three-dimensional structure of the C-terminal fragment of *P. vivax* MSP-1, determined by homology modeling and molecular dynamics refinement. The structural data presented provide a useful comparison between the model of PvMSP-1_{19} and the previously reported structures of this fragment. Corrections reported by Putaporntip et al.[38] for the PvMSP-1 Belem strain sequence described by del Portillo[11] are also discussed.

2. Results and discussion

2.1. Homology modeling of PvMSP-1_{19}

The structure of the C-terminal 19 kDa fragment of PvMSP-1 (Belem strain, Q02569) was obtained from homology modeling simulations. The sequence of PvMSP-1_{19} was aligned with the MSP-1_{19} sequences of which the crystal or solution structures are known; these include *P. cynomolgi*, *P. knowlesi*, and *P. falciparum*. The structure of PcMSP-1_{19} was selected as template to generate the model due to its high sequence identity with that of PvMSP-1_{19}. The alignment reported in Figure 1 revealed a high degree of homology and identity between the different species of *plasmodia*. The alignment of EGF-like domain one, defined from Met-1 to Val-42 for PvMSP-1_{19}, and of domain two, defined from Thr-48 to Ser-91, is observed. Between the Asp-66 and Ser-67 residues there is a segment that is larger in *P. falciparum*. Alignments of the cysteines that typically form the disulfide bonds in the EGF-like domains are also shown.

Five models were generated and inspected. The model showing the best score, as judged by the value of the Modeler objective function, and with the least rms deviation with respect to trace (Cα atoms) of the crystal

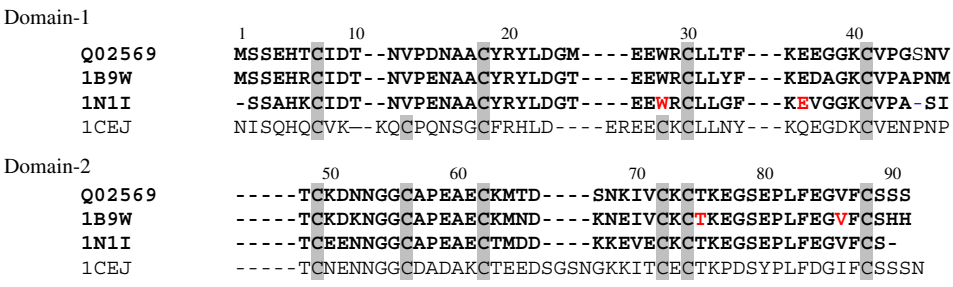

Figure 1. Alignment of the amino acid sequences of MSP-1_{19} from *P. vivax* (Q02569), *P. cynomolgi* (1B9W), *P. knowlesi* (1N1I), and *P. falciparum* (1CEJ). %ID (1B9W, Q02569) = 84; %ID (1N1I, Q02569) = 81; %ID (1CEJ, Q02569) = 54.

structure of PcMSP-1_{19} used as template, was saved for further refinement and validation. The models were also compared between themselves to identify possible variable regions in the PvMSP-1_{19}. These were identified between residues Pro-43 and Val-47, located in the inter-domain linker region and between residues Thr-65 and Lys-69, which belong to the flexible segment in domain two, mentioned above. Additionally, most of the amino acid differences between the C-terminal fragments of the reported protein structures are located in these two regions. In the X-ray structure of PcMSP-1_{19},[35] a unique conformation for the main chain of the hairpin turn could not be proposed, suggesting that this region is highly flexible, a question which was answered in the solution structure of PfMSP-1_{19}.[37] Furthermore, both regions appear to be the most variable ones among different species of *plasmodia*.[40,41]

Further refinement was performed in order to obtain the best conformation on the whole PvMSP-1_{19} structure resulting from Modeler, as described in Section 4. The quality of the refined PvMSP-1_{19} structure thus obtained was checked with ProStat/Structure_Check. The structure satisfied the tests; in the Ramachandran plot, 74.2% of the residues were in the most favored regions. The PvMSP-1_{19} structure superimposes with the PcMSP-1_{19} crystal structure used as template with a rms deviation of 0.7 Å for 79 Cα atoms (Table 1).

2.2. Description of the structure and comparison across species

The overall folding of PvMSP-1_{19} is very similar to that previously reported for other C-terminal fragments of MSP-1 and a comparison was made between the generated model and those structures (Table 1). The structure of PcMSP-1_{19} superimposes on the PvMSP-1_{19} model with the rms mentioned above, the PkMSP-1_{19} structure with an rms deviation of 1.1 Å, whereas the PfMSP-1_{19} structure superimposes with an rms deviation of 3.2 Å. In all cases 79 Cα atoms were considered. The results show the highly similar three-dimensional structures of the molecule.

Figure 2a shows the modeled PvMSP-1_{19} demonstrating the preservation of the structural features of the protein, the disc-shaped form of the molecule with most of their residues accessible to solvent, and the two domains which are structurally related to the EGF motif. Each EGF-like domain contains a major stretch of anti-parallel β-sheet (β1 and β2) including the third and fourth cysteine residues of the EGF motif, and an additional minor anti-parallel β-sheet (β3 and β4) both at the C-terminal end of each domain.

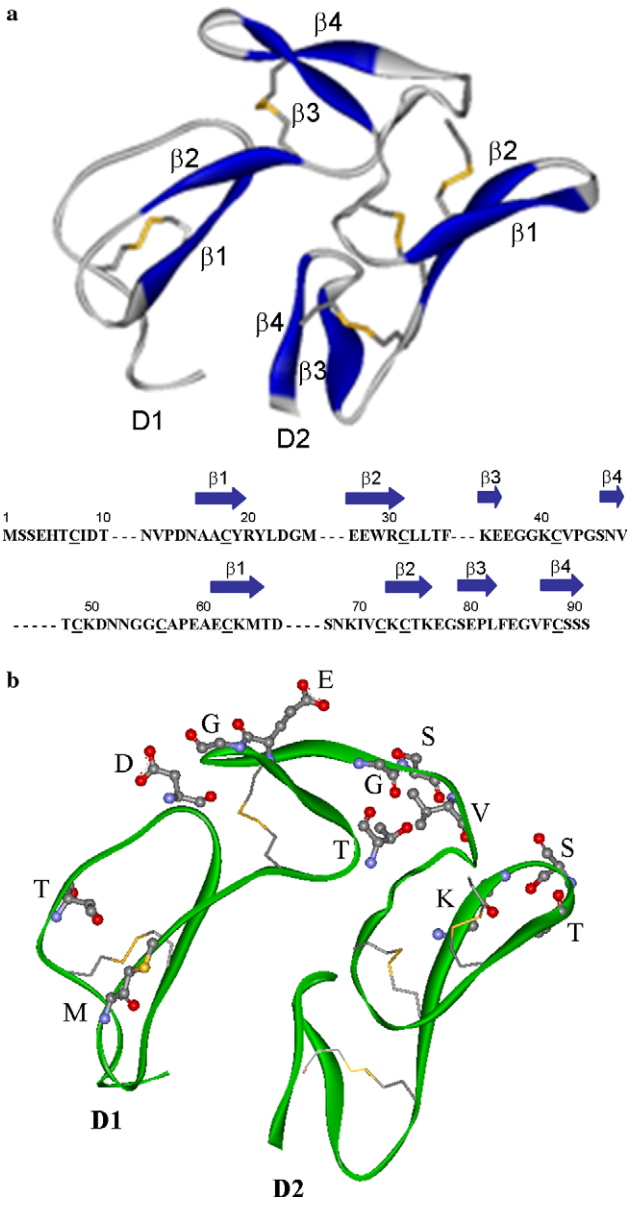

Figure 2. View of the PvMSP-1_{19} model. (a), the PvMSP-1_{19} ribbon representation including disulfide bonds, showing the backbone Cα trace and the anti-parallel β-sheet elements. (b), Variant amino acids (one letter code) are represented in ball and stick side chains, protruding from the main chain represented as a solid ribbon.

Figure 2b shows the variant amino acids between the PcMSP-1_{19} template structure and the derived model

Table 1. Comparison of MSP-1_{19} structures across species

	P. vivax	*P. cynomolgi*	*P. knowlesi*	*P. falciparum*
PDB code		1B9W	1N1I	1CEJ
No. of residues	91	91	92	96
Sequence ID vs *P. vivax*	100%	84%	81%	54%
rms vs *P. vivax*	—	0.7 Å (79 atoms Cα)	1.1 Å (79 atoms Cα)	3.2 Å (79 atoms Cα)
Total area A^2 (Total volume A^3)	5145 (10774)	5706 (10766)	5417 (10566)	5173 (10822)
Ramachandran favored	74.2%	79.8%	77.5%	48.9%

of PvMSP-1_{19}. These amino acid side chains are represented as ball and stick, protruding from the main chain represented as a solid ribbon. The amino acid differences between the proteins occur mainly in the inter-domain region and in the region that corresponds to the flexible hairpin turn. The variability of the latest one was discussed above.

The two EGF domains present in the structure are intimately associated and form a U-shaped structure. The EGF motif is present in a large spectrum of extracellular proteins with widely varying roles in biological processes.[42] Typically, EGF-like domains consist of 40–50 residues with six cysteines in three disulfide bonds with a connectivity of 1–3, 2–4, and 5–6. The 2–4 cysteine is centrally located within the EGF motif, while the 1–3 and 5–6 cysteines secure the N- and C-terminal ends of the domain, respectively. The residues that would form the 2–4 disulfide bridge of the EGF motif are different from cysteine in domain 1 of all *plasmodia* MSP-1_{19}, except for that of *P. falciparum*.[36] The disulfide is replaced with tryptophan and a smaller residue, a valine, isoleucine or threonine. Moreover, of all the independent EGF/laminin-like domain structures currently in the Protein Data Bank,[43] only *Plasmodia* MSP-1_{19} have lost one of its three canonical disulfide bonds. The loss of a structurally important and highly conserved disulfide bond should be most likely due to a functional requirement not yet well understood. Consequently, the two domains of PvMSP-1_{19} model were compared with those present in the crystal and NMR structures available. A comparison of the two domains gives an rms deviation range of 0.6–1.9 Å between equivalent α carbons for domain 1, and 0.7–1.6 Å for domain 2 (Table 2). The domains are similar between the four structures with differences mainly for *P. falciparum*. The two domains of PvMSP-1_{19} model, which have 19% of sequence homology, superimpose with an rms deviation of 3.1 Å for 24 Cα atoms, a value that falls within the structural variability of the EGF motif.

A careful comparison around the residues that substitute cysteines 2 and 4 in domain 1 was performed. The distances between the Cα and Cβ atom pairs in Val-12 and Trp-28 residues that replace cysteines 2 and 4 range between 6.3–6.8 Å and 5.1–5.3 Å, respectively, in the PvMSP-1_{19} model and the reported crystal structures, while the corresponding distances for the 2–4 disulfide bridge present in the PfMSP-1_{19} are 5.2 and 3.3 Å, respectively. These shorter distances afford a compact structure to this domain in PfMSP-1_{19}. However, in spite of the absence of the 2–4 disulfide bridge, the EGF fold is maintained. Superposition of the reported crystal structures with the PvMSP-1_{19} model (Fig. 3a) shows a high similarity around Trp-28. The crystal structures have an amino acid residue bound between Glu-36 and Trp-28, histidine in PkMSP-1_{19} and lysine in PcMSP-1_{19}, while in our model it is absent, in consequence Glu-36 has a different orientation. This region appears to be a main binding pocket, well suited for protein–protein interactions, if we considered that the analysis of the CASTp[39] results show that this is the largest pocket found on our model (154.6 $Å^3$) (Fig. 3b). The residues comprising the pocket of PvMPS-1_{19} are Trp-28, Arg-29, and Cys-30, in β2 strand, Phe-34 in loop, Lys-35 and Glu-36, in β3 strand, Asn-52, Gly-55, and Cys56, in loop, and Val-86 in loop. This region in domain 1 is particularly interesting because of two reasons:

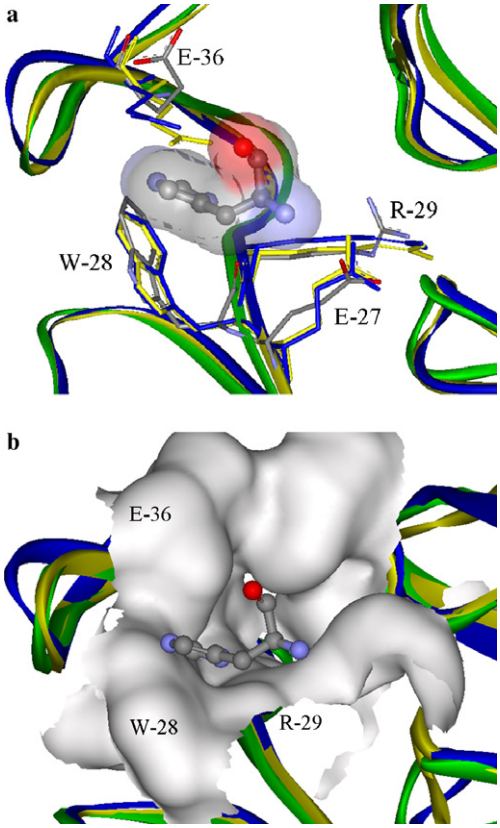

Figure 3. Comparison of the binding pocket between the reported crystal structures PcMSP-1_{19} (yellow line) and PkMSP-1_{19} (blue line) and the PvMSP-1_{19} model (green line). Histidine from the crystal structure from PkMSP-1 is also shown. (a) Cα traces of the three structures superimposed with the side chains shown for residues Glu-27, Trp-28, Arg-29, and Glu-36. (b) The main binding pocket site of PvMSP1_{19}.

Table 2. Comparison of the two MSP-1_{19} domains across species

		P. vivax	*P. cynomolgi*	*P. knowlesi*	*P. falciparum*
PDB code			1B9W	1N1I	1CEJ
rmsd D1 vs D2		3.1 Å (24 atoms Cα)	3.4 Å (24 atoms Cα)	3.6 Å (24 atoms Cα)	4.1 Å (24 atoms Cα)
rmsd vs *P. vivax*	D1		0.6 Å (34 atoms Cα)	0.9 Å (34 atoms Cα)	1.9 Å (34 atoms Cα)
	D2		0.7 Å (42 atoms Cα)	0.8 Å (42 atoms Cα)	1.6 Å (42 atoms Cα)

(1) several growth inhibitory monoclonal antibodies (mAb) bind to the first EGF domain of the PfMSP-1_{19},[44] (2) for some of these antibodies a target epitope has been located on the N-terminal EGF-like domain of the PfMSP-1_{19}.[45]

2.3. Analysis of the corrections to the sequence of PvMSP-1_{19}

The structure of the PvMSP-1_{19} herein described was based on the protein sequence published by del Portillo et al.[11] for the Belem strain. However, to date several corrections to this sequence, some of them within the C-terminal 19 kDa fragment, have been reported.[38] Therefore, the implication of these corrections on the structure of the PvMSP-1_{19} was analyzed. Of the 91 residues, two were substituted, Met-25 with threonine in domain 1, and Gly-44 with alanine in the inter-domain linker region, shown in Figure 4. Met-25 appears to be in a well-structured side chain region, at the beginning of the β2-sheet in domain 1, surface-exposed, and is not involved in interactions across the inter-domain interface. Residue 25, threonine in *P. cynomolgy* and *P. knowlesi*, makes hydrogen bond to main chain amide nitrogen atom of residue Tyr-21. In our model, the hydrogen bond between Met-25 and the corresponding tyrosine residue is also present. Superposition between the PvMSP-1_{19} model and the crystal structures of PcMSP-1_{19} and PkMSP-1_{19} indicated that the displacement of the methionine residue by threonine on the PvMSP-1_{19} model can be performed with minimum perturbation of the conformation in domain 1 of PvMSP-1_{19} and the side chain of threonine could account for a similar orientation as that of methionine (Fig. 5a). The second displacement, Gly-44 with alanine, is conservative and occurs in the extended polypeptide segment that makes the transition from domain 1 to domain 2. In the crystal structures of PcMSP-1_{19} and PkMSP-1_{19}, a hydrogen bond is present between residue 44, alanine in both structures, and residue 33, tyrosine in *P. cynomolgy* and glycine in *P. knowlesi*. The displacement mentioned above apparently does not disturb the ability to make hydrogen bond between residue 44 and the side

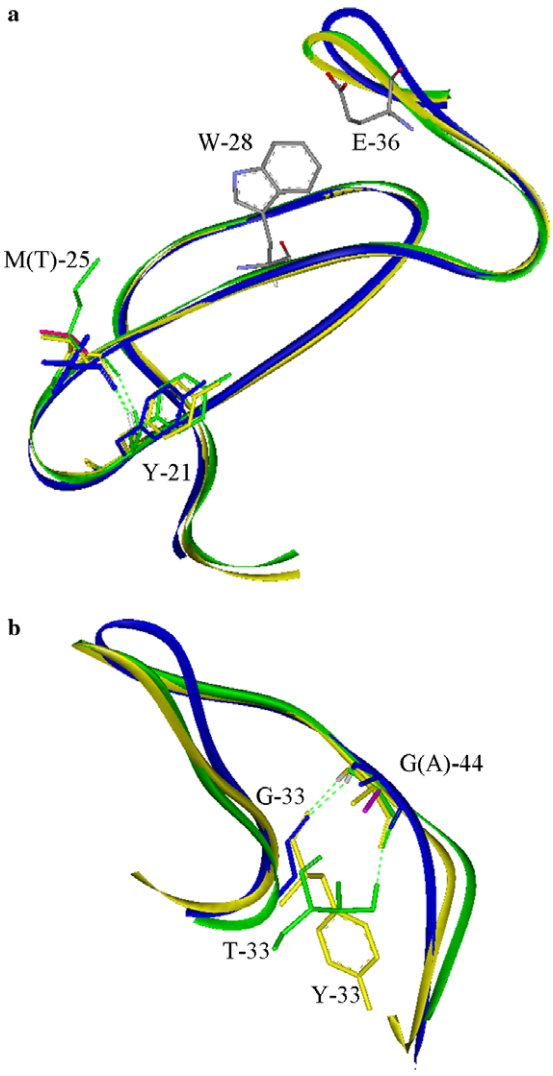

Figure 5. Superposition of PvMSP-1_{19} (green line) onto PcMPS-1_{19} (yellow line) and PkMSP-1_{19} (blue line). (a) Segment around Met-25 and (b) around Gly-44. Displacements by Thr-25 and Ala-44 on the PvMSP-1_{19} model are shown in pink.

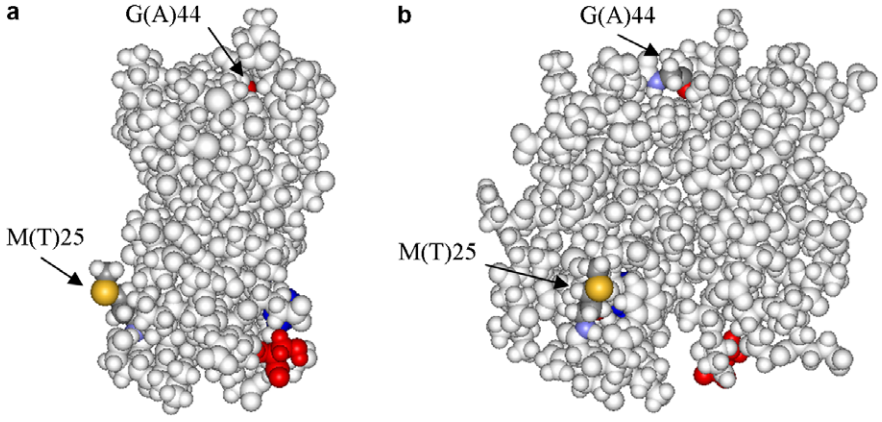

Figure 4. CPK model of PvMSP-1_{19}, showing the location of the corrections reported by Putaporntip[38] on the original PvMSP-1 sequence described for the Belem strain. Corrections are explained in the text and residues between parentheses correspond to that reported by Putaporntip. (a) Lateral view (b) Front view. C-terminal Ser-91 displayed in red.

chain of Thr-33 in the PvMSP-1_{19} structure (Fig. 5b). These results may be considered for further experimental studies on identification of potential B-cell epitopes.

3. Conclusions

The three-dimensional structure of the C-terminal 19 kDa fragment of *P. vivax* MSP-1 was built by using the homology modeling based on the known crystal structure of *P. cynomolgy* MSP-1_{19}. Then, the model structure was refined by energy minimization and molecular dynamics methods. Our model reveals the presence of a main binding pocket in domain 1, well suited for protein–protein interactions. Corrections reported by Putaporntip et al.[38] for the PvMSP-1 Belem strain sequence described by del Portillo et al.[11] were also inspected, and corrections can be introduced with minimum perturbation of the conformation in domain 1 and in the extended polypeptide segment that makes the transition from domain 1 to domain 2. The model thus obtained, the analysis of the potential hydrophilic regions, corrections to the sequence, and the proposed main binding pocket in domain 1, are under consideration for the identification of several potential B-cell epitopes. Studies are under way to examine interaction between relevant peptides and antibodies from individuals largely exposed to *P. vivax* malaria.

4. Theory and methods

Modeling studies as well as the generation and analysis of the structures were performed on a Silicon Graphics Indigo 2 workstation. The modeling, calculation of energy minimization, molecular dynamics, and analysis of the three-dimensional models were performed using Insight II, the Modeler, Discover, Analysis, and Decipher packages (Molecular Simulations Inc., Walthman, M.A.). The CASTp[39] server was used for identification of the binding site. Molecular figures were prepared using the Insight II and WebLab ViewerLite 3.20. The program DeepView/SwissPdb-Viewer 3.7 (Glaxo-SmithKline) was also used.

4.1. 3D model building

Sequence alignment between C-terminal fragments of PfMSP-1, PkMSP-1, PcMSP-1 (PDB codes 1CEJ, 1N1I, and 1B9W, respectively), and PvMSP-1 (Belem strain) (TrEMBL Accession No. Q02569, GenBank Accession No. AAA63427.1) was generated with the structural alignment tool of the Modeler module of Insight II and corrected manually until a satisfactory placement of conserved blocks and amino acid identities was achieved. The 10 invariant cysteines that would form disulfide bridges of the EGF motifs in PkMSP-1_{19},[36] PcMSP-1_{19},[35] and PvMSP-1_{19}[11] were considered as restraints when generating the models. Five conformers were generated with Modeler/Insight II using the C-terminal fragment of the PcMSP-1_{19} as template. The models were then analyzed with ProStat/Structure_Check. Decipher was used to generate Ramachandran plots. The best model was used as starting structure for a further refinement. The reported corrections[38] to the PvMSP-1_{19} Belem sequence published by del Portillo et al.[11] were also evaluated.

4.2. Model refinement and evaluation

For energy refinement with Discover, hydrogen atoms were added to the model according to pH 7 and partial charges were assigned to all atoms. The calculations were performed by the Discover module of Insight II using the consistent-valence force field (CVFF), with a 20 Å cut-off distance for non-bonded interactions and a dielectric constant of 1. The best model obtained by Modeler was surrounded by a 5 Å water shell and energy minimized in order to make it able to undergo molecular dynamics (MD) simulation.

The water molecules were minimized, while holding de PvMSP-1_{19} fixed, by the steepest descent method, followed by conjugated gradient minimization down to 1 kcal mol^{-1} Å^{-1}. After this first step, constraints with a force constant of 1000 kcal mol^{-1} Å^{-2} were applied to the backbone atoms (N, Cα, C, O) and gradually decreased from 1000 to 2 kcal mol^{-1} Å^{-2}. Conjugated gradient minimizations were carried out until 0.5 kcal mol^{-1} Å^{-1} of convergence on the gradient. Finally, the last step of minimization was performed without any constraints. Subsequently, MD simulations were carried out at 300 K. The system was allowed to equilibrate, followed by a 5 ps molecular dynamics run at 300 K. At the end of the MD simulation, the structure was once again minimized using conjugated gradient energy minimization until the root mean-square (rms) gradient energy was lower than 0.1 kcal mol^{-1} Å^{-1}.

The final model was checked with ProStat. The ProStat module of Insight II identifies and lists the number of instances where structural features differ significantly from the average values calculated from known proteins.

4.3. Identification of the binding site of PvMSP-1_{19}

In this study, the CASTp[39] server was used for the identification of the main binding site in our model of PvMSP-1_{19}. CASTp provides identification and analytical measurements of surface accessible pockets, for proteins and other molecules, which can be used to guide protein–protein interactions. Through comparison of the reported structures of *P. cynomolgi*, *P. knowlesi*, and *P. falciparum*, we can predict the main binding site of PvMSP-1_{19}.

Acknowledgments

We thank the Instituto de Investigaciones Farmacéuticas and the Consejo de Desarrollo Científico y Humanístico of the Universidad Central de Venezuela (UCV) and the Instituto Venezolano de Investigaciones Científicas (IVIC) for partial financial support. We also thank Dr. Werner Wilbert, of the Department of

Anthropology of the Instituto Venezolano de Investigaciones Científicas (IVIC), for his kind review of the manuscript.

References and notes

1. Breman, J. G. *Am. J. Trop. Med. Hyg.* **2001**, *64*, 1.
2. Mendis, K.; Sina, B. J.; Marchesini, P.; Carter, R. H. *Am. J. Trop. Med. Hyg.* **2001**, *64*, 97.
3. Holder, A. A.; Lockyer, M. J.; Odink, K. G.; Sandhu, J. S.; Riveros-Moreno, V.; Nicholls, S. C.; Hilman, Y.; Dayey, L. S.; Tizard, M. L.; Schwarz, R. T.; Freeman, R. R. *Nature* **1985**, *317*, 270.
4. Smythe, J. A.; Coppel, R. L.; Brown, G. V.; Ramasamy, R.; Kemp, D. J.; Anders, R. F. *Proc. Natl. Acad. Sci. U.S.A.* **1988**, *85*, 195.
5. Marshall, V. M.; Silva, A.; Foley, M.; Cranmer, S.; Wang, L.; McColl, D. J.; Kemp, D. J.; Coppel, R. L. *Infect. Immun.* **1997**, *6*, 4460.
6. Trucco, C.; Fernandez-Reyes, D.; Howell, S.; Stafford, W. H.; Scott-Finnigan, T. J.; Grainger, M.; Ogun, S. A.; Taylor, W. R.; Holder, A. A. *Mol. Biochem. Parasitol.* **2001**, *112*, 91.
7. Pachebat, J. A.; Ling, I. T.; Grainger, M.; Trucco, C.; Howell, S.; Fernandez- Reyes, D.; Gunaratne, R.; Holder, A. A. *Mol. Biochem. Parasitol.* **2001**, *117*, 83.
8. Black, C. G.; Wu, T.; Wang, L.; Hibbs, A. R.; Coppel, R. L. *Mol. Biochem. Parasitol.* **2001**, *114*, 217.
9. Stahl, H. D.; Bianco, A. E.; Crewther, P. E.; Anders, R. F.; Kyne, A. P.; Coppel, R. L.; Mitchell, G. F.; Kemp, D. J.; Brown, G. V. *Mol. Biol. Med.* **1986**, *3*, 351.
10. Black, C. G.; Wang, L.; Wu, T.; Coppel, R. L. *Mol. Biochem. Parasitol.* **2003**, *127*, 59.
11. del Portillo, H. A.; Longacre, S.; Khouri, E.; David, P. H. *Proc. Natl. Acad. Sci. U.S.A.* **1991**, *88*, 4030.
12. Barnwell, J. W.; Galinski, M. R.; DeSimone, S. G.; Perler, F.; Ingravallo, P. *Exp. Parasitol.* **1999**, *91*, 238.
13. Galinski, M. R.; Corredor-Medina, C.; Povoa, M.; Crosby, J.; Ingravallo, P.; Barnwell, J. W. *Mol. Biochem. Parasitol.* **1999**, *101*, 131.
14. Black, C. G.; Barnwell, J. W.; Huber, C. S.; Galinski, M. R.; Coppal, R. L. *Mol. Biochem. Parasitol.* **2002**, *120*, 215.
15. Vargas-Serrato, E.; Barnwell, J. W.; Ingravallo, P.; Perler, F. B.; Galinski, M. R. *Mol. Biochem. Parasitol.* **2002**, *120*, 41.
16. Perez-Leal, O.; Sierra, A. Y.; Barrero, C. A.; Moncada, C.; Martinez, P.; Cortes, J.; Lopez, Y.; Torres, E.; Salazar, L. M.; Patarroyo, M. A. *Biochem. Biophys. Res. Commun.* **2004**, *324*, 1393.
17. Perez-Leal, O.; Sierra, A. Y.; Barrero, C. A.; Moncada, C.; Martinez, P.; Cortes, J.; Lopez, Y.; Salazar, L. M.; Hoebeke, J.; Patarroyo, M. A. *Biochem. Biophys. Res. Commun.* **2005**, *331*, 1178.
18. Egan, A. F.; Blanckman, M. J.; Kaslow, D. C. *Infect. Immun.* **2000**, *68*, 1418.
19. Stowers, A. W.; Cioce, V.; Shimp, R. L.; Lawson, M.; Hui, G.; Muratova, O.; Kaslow, D. C.; Robinson, R.; Long, C. A.; Miller, L. H. *Infect. Immun.* **2001**, *69*, 1536.
20. Blackman, M. J.; Ling, I. T.; Nicholls, S. C.; Holder, A. A. *Mol. Biochem. Parasitol.* **1991**, *49*, 29.
21. Blackman, M. J.; Chappel, J. A.; Shai, S.; Holder, A. A. *Mol. Biochem. Parasitol.* **1993**, *62*, 103.
22. Holder, A. A.; Sandhu, J. S.; Hillman, Y.; Davey, L. S.; Nicholls, S. C.; Cooper, H.; Lockyer, M. J. *Parasitology* **1987**, *94*, 199.
23. Blackman, M. J.; Heidrich, H. G.; Donachie, S.; McBride, J. S.; Holder, A. A. *J. Exp. Med.* **1990**, *172*, 379.
24. Blackman, M. J.; Holder, A. A. *Mol. Biochem. Parasitol.* **1992**, *50*, 307.
25. Blackman, M. J.; Scott-Finnigan, T. J.; Shai, S.; Holder, A. A. *J. Exp. Med.* **1994**, *180*, 389.
26. Gozalo, A.; Lucas, C.; Cachay, M.; Wellde, B. T.; Hall, T.; Bell, B.; Wood, J.; Watts, D.; Wooster, M.; Lyon, J. A.; Moch, J. K.; Haynes, J. D.; Williams, J. S.; Holland, C.; Watson, E.; Kester, K. E.; Kaslow, D. C.; Ballou, W. R. *Am. J. Trop. Med. Hyg.* **1998**, *59*, 991.
27. Chang, S. P.; Gibson, H. L.; Lee-Ng, C. T.; Barr, P. J.; Hui, G. S. *J. Immunol.* **1992**, *149*, 548.
28. Kumar, S.; Yadava, A.; Keister, D. B.; Tian, J. H.; Ohl, M.; Perdue-Greenfield, K. A.; Miller, L. H.; Kaslow, D. C. *Mol. Med.* **1995**, *1*, 325.
29. Kumar, S.; Collins, W.; Egan, A.; Yadava, A.; Garraud, O.; Blackman, M. J.; Guevara-Patiño, J. A.; Diggs, C.; Kaslow, D. C. *Infect. Immun.* **2000**, *68*, 2215.
30. Collins, W. E.; Kaslow, D. C.; Sullivan, J. S.; Morris, C. L.; Galland, G. G.; Yang, C.; Saekhou, A. M.; Xiao, L.; Lal, A. A. *Am. J. Trop. Med. Hyg.* **1999**, *60*, 350.
31. Yang, C.; Collins, W. E.; Sullivan, J. S.; Kaslow, D. C.; Xiao, L.; Lal, A. A. *Infect. Immun.* **1999**, *67*, 342.
32. Sierra, A. Y.; Barrero, C. A.; Rodriguez, R.; Silva, Y.; Moncada, C.; Vanegas, M.; Patarroyo, M. A. *Vaccine* **2003**, *21*, 4133.
33. Soares, I. S.; Levitus, G.; Sousa, J. M.; Del Portillo, H. A.; Rodrigues, M. M. *Infect. Immun.* **1997**, *65*, 1606.
34. Udhayakumar, V.; Anyona, D.; Kariuki, S.; Shi, Y. P.; Bloland, P. B.; Branch, O. H.; Weiss, W.; Nahlen, B. L.; Kaslow, D. C.; Lal, A. A. *J. Immunol.* **1995**, *154*, 6022.
35. Chitarra, V.; Holm, I.; Bentley, G. A.; Pêtres, S.; Longacre, S. *Mol. Cell* **1999**, *3*, 457.
36. Garman, S. C.; Simcoke, W. N.; Stowers, A. W.; Garboczi, D. N. *J. Biol. Chem.* **2003**, *278*, 7264.
37. Morgan, W. D.; Birdsall, B.; Frenkiel, T. A.; Gradwell, M. G.; Burghaus, P. A.; Syed, S. E. H.; Uthaipibull, C.; Holder, A. A. *J. Mol. Biol.* **1999**, *289*, 113.
38. Putaporntip, C.; Jongwutiwes, S.; Sakihama, N.; Ferreira, M. U.; Kho, W. G.; Kaneko, A.; Kanbara, H.; Hattori, T.; Tanabe, K. *Proc. Natl. Acad. Sci. U.S.A.* **2002**, *99*, 16348.
39. Binkowski, T. A.; Naghibzadeg, S.; Liang, J. *Nucleic Acid Res.* **2003**, *31*, 3352.
40. Holder, A. A.; Blackman, M. J.; Burgnaus, P. A.; Chappel, J. A.; Ling, I. T.; McCallum-Deighton, N.; Sahi, S. *Mem. Inst. Oswaldo Cruz* **1992**, *87*(Suppl. III), 37.
41. Daly, T. M.; Burns, J. M.; Long, C. A. *Mol. Biochem. Parasitol.* **1992**, *52*, 279.
42. Campbell, I. D.; Bork, P. *Curr. Opin. Struct. Biol.* **1993**, *3*, 385.
43. Berman, H. M.; Westbrook, J.; Feng, Z.; Gilliland, G.; Bhat, T. N.; Weissig, H.; Shindyalov, I. N.; Bourne, P. E. *Nucleic Acids Res.* **2000**, *28*, 235.
44. Chappel, J. A.; Holder, A. A. *Mol. Biochem. Parasitol.* **1993**, *60*, 303.
45. Pizarro, J. C.; Chitarra, V.; Verger, D.; Holm, I.; Pêtres, S.; Dartevelle, S.; Nato, F.; Longacre, S.; Bentley, G. A. *J. Mol. Biol.* **2003**, *328*, 1091.